Plant, Cell and Environment (2005) **28**, 800–812

Inter-vessel pitting and cavitation in woody Rosaceae and other vesselled plants: a basis for a safety versus efficiency trade-off in xylem transport

JAMES K. WHEELER, JOHN S. SPERRY, UWE G. HACKE & NGUYEN HOANG

Department of Biology, University of Utah, Salt Lake City UT 84112, USA

ABSTRACT

The hypothesis that greater safety from cavitation by air-seeding through inter-vessel pits comes at the cost of less porous pit membranes with greater flow resistance was tested . Sixteen vessel-bearing species were compared: 11 from the Rosaceae, four from other angiosperm families, and one fern. Unexpectedly, there was no relationship between pit resistance (and hence the prevailing membrane porosity) and cavitation pressure. There was, however, an inverse relationship between pit area per vessel and vulnerability to cavitation ($r^2 = 0.75$). This suggests that cavitation is caused by the rare largest membrane pore per vessel, the average size of which increases with total pit area per vessel. If safety from cavitation constrains pit membrane surface area, it also limits vessel surface area and the minimum vessel resistivity. This trade-off was consistent with an approximately three-fold increase in vessel resistivity with cavitation pressure dropping from –0.8 to –6.6 MPa. The trade-off was compensated for by a reduction in the percentage of vessel wall pitted: from 10–16% in vulnerable species to 2–4% in resistant species. Across species, end-wall pitting accounted for 53 ± 3% of the total xylem resistivity. This corresponded to vessels achieving on average 94 ± 2% of their maximum possible conductivity if vessel surface area is constrained.

Key-words: air-seeding; cavitation resistance; pit resistance; vessel length; water transport; xylem flow resistance; xylem structure and function.

INTRODUCTION

'Safe' xylem transport means sufficient protection against conduit blockage, primarily from cavitation and embolism. 'Efficient' transport means low flow resistance for a given investment in vascular tissue. It has long been thought that there is a structural trade-off between these two traits: that efficient xylem comes at the cost of being vulnerable to failure (Zimmermann 1983; Tyree, Davis & Cochard 1994; Martinez-Vilalta *et al*. 2002). Two observations suggest the trade-off. For one, there is a tendency for plants that experience more cavitation-inducing stress to possess more cavitation-resistant xylem, and vice-versa (Davis *et al*. 1999; Hacke, Sperry & Pittermann 2000; Pockman & Sperry 2000). Minimum safety margins from cavitation are similarly small across the spectrum (Sperry 1995). If cavitation resistance came at no cost to the plant, safety margins would seemingly be huge and cavitation rare. Second, there is a tendency for the hydraulic resistivity of xylem on a cross-sectional area basis (pressure gradient divided by flux density) to increase with increasing cavitation resistance. This is mirrored by a trend of narrower xylem conduits in safer xylem (Martinez-Vilalta *et al*. 2002). 'Trend' is the appropriate term because the relationship is noisy and may or may not be statistically significant depending on the species sampled (Tyree *et al*. 1994; Hacke & Sperry 2001).

What could be the cause of a trade-off? The answer is simple for resistance to freezing-induced cavitation. Wider conduits, whether tracheids or vessels, appear to be more vulnerable to freezing-induced cavitation than narrower ones (Ewers 1985; Pittermann & Sperry 2003). This is consistent with wider conduits containing more air in solution per length of conduit, and hence forming larger air bubbles during ice formation. Larger air bubbles nucleate cavitation at less negative pressures during thaw. Narrower conduits are thus safer from freezing-induced cavitation, but also less efficient in transporting water per cross-sectional area.

This paper concerns the more complex question of an efficiency trade-off with safety from water-stress induced cavitation. There is considerable evidence that the cause of cavitation by negative pressure is the failure of the pit 'valves' between conduits (Crombie, Hipkins & Milburn 1985; Cochard, Cruiziat & Tyree 1992; Salleo *et al*. 1996; Sperry *et al*. 1996). These pits prevent air in already damaged conduits from entering functional ones and 'air-seeding' cavitation. Accordingly, any trade-off between safety and efficiency should depend on the functioning of these valves.

Based on a modelling study of the valve action of pits we proposed that an air-tight pit comes at the cost of high flow resistance through the pit (Sperry & Hacke 2004). For a uniformly porous ('homogenous') pit membrane typical of

Correspondence. John S. Sperry. Fax: +1 801 581 4668; e-mail: sperry@biology.utah.edu

angiosperms and many seedless vascular plants (as opposed to the torus-margo organization of many conifer pits), the air-seeding pressure (P) through pre-existing pores can be predicted by the capillary equation: $P = -4T/d$, where T is the surface tension of water and d is the diameter of the largest membrane pore in the conduit. Greater safety from air-seeding requires a smaller maximum pore diameter per conduit. If the average porosity of the membrane is correlated with the maximum pore diameter, the flow resistance through the membrane should increase with increasing air-seeding protection, because flow resistance through pores in a thin membrane is inversely proportional to the pore diameter raised to the third power (equation 15 in Sperry & Hacke 2004).

Here we test this hypothesis by estimating the flow resistance through pits of species with widely varying resistance to cavitation by water stress. We limited our study to inter-vessel pits with homogenous pit membranes and to pits without vestures, recognizing that vestures, torus-margo membranes, or other modifications may represent qualitatively different solutions to a trade-off. We sampled intensively within a single family (Rosaceae) to minimize qualitative differences that might occur even within the homogenous type of pit membrane between diverse clades. For broader representation we also sampled a smaller number of disparate angiosperm families as well as a vessel-bearing fern. Many of the necessary measurements had already been made on these species from a related study (Sperry, Hacke & Wheeler, 2005), making it natural to include them.

A trade-off at the pit level does not necessarily translate to a trade-off at the whole conduit or xylem level. If the diameter and length of a vessel is uncoupled from the air-seeding properties of its pits, safe xylem does not necessarily have to be inefficient. High-resistance pits can be placed in wide and long conduits that render any pit bottleneck negligible (Sperry & Hacke 2004). However, our recent work suggests that this does not happen. Across very diverse xylem types we found that approximately 50% of the xylem flow resistivity is attributable to interconduit pits (Sperry *et al*. 2005). For an unknown reason, vessels are not long enough to compensate for their end wall resistance. A large end wall resistivity is consistent with a linkage between air-seeding pressure and conduit size, an issue we consider in detail in this investigation.

MATERIALS AND METHODS

Plant material

Eleven species of native Rosaceae of diverse habitat and growth form (Table 1) were collected from a variety of locales in the Wasatch Mountains near Salt Lake City, Utah. Each species was collected from a single limited population to minimize variation. Stems were cut, wrapped in plastic bags, and brought to the laboratory. Five other species from the related study (Table 1) included native and cultivated species of diverse families that were collected locally as described elsewhere (Sperry *et al*. 2005).

Vulnerability curves

The centrifuge method was used for measuring vulnerability to water-stress induced cavitation. Stems 14.2 cm long

Table 1. Study species, their symbols used in figures, and associated measurements not in figures

Species and figure symbol		Contact fraction	Pitfield fraction	Length fraction	L'/L	r_P (MPa s m^{-1})
Amelanchier alnifolia M. Roemer	Aa	0.14 ± 0.018	0.37 ± 0.020	0.41 ± 0.11	0.80 ± 0.09	626 ± 183
A. utahensis Koehne	Au	0.13 ± 0.008	0.33 ± 0.020	0.40 ± 0.05	0.80 ± 0.04	112 ± 35
Cercocarpus ledifolius Torr. & Gray	Cl	0.05 ± 0.008	0.44 ± 0.018	0.16 ± 0.06	0.92 ± 0.14	39 ± 14
C. montanus Raf.	Cm	0.06 ± 0.002	0.26 ± 0.009	0.18 ± 0.05	0.91 ± 0.10	60 ± 12
Holodiscus dumosus (Hook.) Heller.	Hd	0.07 ± 0.006	0.44 ± 0.063	0.19 ± 0.06	0.91 ± 0.11	328 ± 84
Physocarpus malvaceus (Greene) Kuntze	Pm	0.08 ± 0.008	0.50 ± 0.036	0.23 ± 0.09	0.89 ± 0.14	337 ± 104
Purshia tridentata (Pursh) DC.	Pt	0.08 ± 0.007	0.28 ± 0.012	0.21 ± 0.04	0.89 ± 0.08	84 ± 24
Rosa nutkana C. Presl	Rn	0.10 ± 0.013	0.46 ± 0.025	0.25 ± 0.09	0.88 ± 0.13	276 ± 75
Rubus leucodermis Torr. & Gray	Rl	0.15 ± 0.011	0.53 ± 0.008	0.37 ± 0.06	0.81 ± 0.05	285 ± 120
R. parviflorus Nutt.	Rp	0.19 ± 0.006	0.43 ± 0.018	0.42 ± 0.05	0.79 ± 0.04	78 ± 15
Sorbus scopulina Greene	Ss	0.10 ± 0.011	0.39 ± 0.033	0.30 ± 0.13	0.85 ± 0.16	205 ± 73
Vitis vinifera L. (Vitaceae)	VV	0.14 ± 0.015	0.75 ± 0.111	0.33 ± 0.13	0.83 ± 0.13	168 ± 63
Sambucus caerulea Raf. (Adoxaceae)	SC	0.25 ± 0.024	0.56 ± 0.025	0.54 ± 0.08	0.73 ± 0.05	371 ± 92
Acer negundo L. (Aceraceae)	AN	0.15 ± 0.011	0.63 ± 0.018	0.42 ± 0.06	0.79 ± 0.06	66 ± 15
Salix exigua Nutt. (Salicaceae)	SE	0.22 ± 0.006	0.73 ± 0.013	0.44 ± 0.04	0.78 ± 0.05	72 ± 19
Pteridium aquilinum (L) Kuhn (Polypodiaceae)	PA	0.35 ± 0.013	0.22 ± 0.017	1.0 ± 0.0	0.5 ± 0	31 ± 7

The five species from families other than the Rosaceae are listed last. Double capital symbols distinguish these non-Rosaceae species in figures. 'Contact fraction' is the portion of the vessel wall area in contact with an adjacent vessel. 'Pitfield fraction' is the portion of the interconduit pitfield occupied by pits. The product of these two fractions gives the 'pit fraction' (F_P), the total pit area per vessel area. 'Length fraction' is the fraction of the total vessel length contacting adjacent vessels. The ratio L'/L (Fig. 1) was calculated from the length fraction and average vessel length. Grand means from four to six stems per species ± SE.

and 1–5 years of age were flushed with a filtered (0.2 μm) 20 mM KCl at approximately 0.1 MPa to remove native embolism. The 20 mM KCl solution was used to control for any ion effect on pit membrane conductivity (Ieperen, Meeteren & Gelder 2000; Zwieniecki, Melcher & Holbrook 2001b). Flushed stems were spun on a custom-built rotor (Alder *et al*. 1997) to progressively more negative pressure, with their hydraulic conductivity (flow rate per pressure gradient) being measured between spins to assess the loss in conductivity from cavitation. A Weibull function (Neufeld *et al*. 1992) was fitted to the conductivity versus negative pressure relationship for each stem, and the pressure inducing 50% loss of conductivity calculated. We refer to the absolute value of this pressure as the 'P_{50}' and use it to represent the safety of the xylem from water-stress-induced cavitation. A minimum of six stems per species were used to obtain the average P_{50} for each species.

The conductivity was measured by fitting the stem to tubing filled with the filtered KCl solution. A gravity-induced pressure difference across the stem drove flow into a reservoir on an electronic balance. Stems generally absorbed a small amount of water in the absence of applied pressure. This negative flow was subtracted from the flow under pressure to obtain the net pressure-driven flow rate. The net flow rate was divided by the pressure gradient to obtain the conductivity.

Methodology of determining area-specific pit resistance (r_P)

We estimated inter-vessel pit resistance using an approach similar to Schulte & Gibson's (1988) study on tracheids (see also Lancashire & Ennos 2002). The pit resistance was determined from flow measurements through stem segments and the dimensions of the vessels and pits in the segments. The method assumes the xylem of a stem can be represented by longitudinal files of overlapping vessels of average size (Fig. 1). Lumen and end-wall are arranged in series with a unit length of L' (Fig. 1), which is shorter than the vessel length (L) by one end wall. The average vessel resistivity (R_C, pressure gradient divided by volume flow rate) is the sum of the lumen (R_L) and end wall (R_W) resistivity for the average-sized vessel. The end-wall resistivity (like any resistivity) is a length-independent measure that equals the end wall resistance (r_W, pressure divided by volume flow rate) divided by the length L' between successive end walls. Measuring L' thus yields the end wall resistance: $r_W = R_W L'$. The end wall resistance itself is a function of the extent of the end wall – more specifically the number and area of pits it contains. From measurements of the area of pits in one end wall, the end wall resistance can be converted to a pit resistance on an area basis ($r_P = r_W \times$ pit area). The cavitation pressure of the average vessel corresponding to the resistance measurements was assumed to be near the P_{50}, allowing safety from cavitation to be compared with flow resistances. Tables 1 and 2 summarize the major variables used in the analysis.

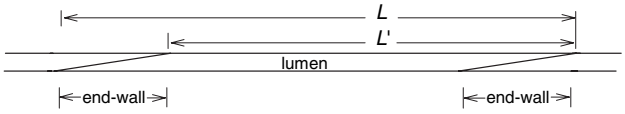

Figure 1. Vessel geometry assumed for calculation of end wall and pit resistances. Stem xylem of each species was represented by longitudinal files of vessels of average length, diameter, and end-wall overlap. A portion of one of many parallel files is shown. The length L' is the length of the longitudinally repeating unit of lumen plus end wall. It is shorter than the total vessel length by one end wall. The end wall resistance (r_W) is the end wall resistivity multiplied by L'. The area-specific pit resistance (r_P) is the r_W divided by the pit area in one end-wall, which was assumed to be half of the total pit area per vessel. End wall and pit resistances represent maximum values because the calculation does not account for any lateral pitting between parallel files of vessels.

Anatomical measurements were made using IMAGE PRO PLUS (Media Cybernetics Inc., Silver Springs, MD, USA) and IMAGEJ software (free-ware available from http://rsb.info.nih.gov/ij/). An overview of calculations is provided in the Appendix. The parameters R_C, R_L, R_W, and F_W (below) were already available for the non-Rosaceae species using an analogous methodology (Sperry *et al*. 2005).

Vessel lengths (L)

Stems were flushed to remove native embolism and injected with silicone (Rhodorsil RTV-141; Rhodia USA, Cranbury, NJ, USA; imported by Walco Materials, Escondido, CA, USA) coloured with red pigment (Silastic LSPRD11; Dow Corning, Kendallville, IN, USA) at 0.5 MPa for 1 h before curing in an oven for approximately 1 h at 70 °C. Earlier work indicated that this silicone does not penetrate pit membranes (André 2002) and fills the vessels completely, making them easier to recognize than the traditional paint pigment injection (Sperry *et al*. 2005). The cured stems were cut at several distances from the injection surface, and the average number of silcone-filled vessels per xylem area was counted. Most vessels were short (Zimmermann & Jeje 1981), so we used an exponential scale to concentrate the vessel counts near the injection surface

$$L_i = L_{min}(L_{min}/L_{max})^{(i-1)/(N-1)} \quad (1)$$

where L_i is the ith distance counted starting at $i = 1$ at L_{min}, which was the shortest non-zero distance (0.005 m) and ending at $i = N$ for L_{max}, which was the longest length counted. The L_{min} was constant at 0.005 m, whereas L_{max} was varied according the vessel length of the species.

Rather than using the double-difference algorithm (Zimmermann 1983) for calculating vessel lengths we extended the approach originated by Cohen, Bennick & Tyree (2003). An exponential decay function was fitted to the decrease in density of silicone-filled vessels (N_L) with distance L from the injection surface:

$$N_L = N_0 e^{(-kL)} \quad (2)$$

Table 2. List of major variables with definition and units employed

Symbol	Definition	Units employed
A_P	surface area of inter-vessel pit membranes	mm^2
A_V	total surface area of vessel wall	mm^2
F_P	'pit fraction' = A_P/A_V	–
F_W	'end wall fraction' = R_W/R_C	–
L	vessel length (Fig. 1)	m
L'	length between vessel end walls (Fig. 1)	m
P_{50}	absolute value of xylem pressure causing 50% loss of hydraulic conductivity	MPa
R_C	vessel resistivity	MPa s mm^{-4}
R_L	lumen resistivity	MPa s mm^{-4}
R_W	end wall resistivity	MPa s mm^{-4}
R_{Ca}	vessel resistivity on lumen area basis	MPa s m^{-2}
r_W	resistance of one vessel end wall	MPa s mm^{-3}
r_P	resistance of inter-vessel pits on pit area basis	MPa s m^{-1}

A 'resistivity' (R) is length-independent (pressure gradient per volume flow rate) and may be further standardized by cross-sectional area of flow as in the R_{Ca} term. A 'resistance' (r) is length-dependent (pressure difference per volume flow rate) but may be standardized by cross-sectional area of flow as in the r_P term.

where N_0 is the total vessel density and k the best fit extinction coefficient. The fraction of conduits of length L (P_L) is given by L/N_0 times the second derivative of Eqn 2

$$P_L = Lk^2 e^{(-kL)} \quad (3)$$

Integrating the product of P_L and L over the length distribution ($\int P_L L \, dL$ from $L = 0$ to infinity) gives the mean vessel length. As the length distributions were short-skewed, the mean of the log-transformed length distribution was used to represent the average-sized vessel (Fig. 1, L). Each species was represented by the grand mean of three to seven stems. Vessel lengths were already available for the five non-Rosaceae species using similar methods (Sperry *et al*. 2005). (Note: Eqn 3 incorrect in Sperry *et al*. 2005 as Eqn 2.)

Conduit (R_C), lumen (R_L), and end wall (R_W) resistivities

The R_C was measured on stems that were longer than the vast majority of the vessels. Measured stems were 14 cm and longer than 96% of the vessels for all species except *Holodiscus dumosus*. Open vessels in stem segments will cause R_C to be under-estimated, but by less than 7% (even in *H. dumosus*) assuming the linear relationship between R and open vessel percentage observed in the related study (Sperry *et al*. 2005). Stems were flushed to remove native embolism and their resistivity measured with the same apparatus that was used for vulnerability curve measurement. The stem was then perfused with basic fuchsin (0.1% w/w) or safranin (0.1% w/w) to mark the functional xylem. The resistivity was multiplied by the stained xylem area to obtain the xylem area-specific resistivity. This was multiplied by the vessel density of the same stem to obtain the R_C of the average vessel. To assess the conducting efficiency of vessels across species, R_C was also expressed on the basis of the cross-sectional area of a lumen of average diameter as calculated in the following paragraph (R_{ca}; Table 2).

The same stem was sectioned and the lumen resistivity (R_L) estimated from vessel diameter measurements. The area of each vessel lumen in a radial sector of functional xylem was measured, and the equivalent circle diameter calculated before summing the Hagen–Poiseuille conductivities to obtain the total conductivity per area of the radial sector. Several sectors per stem (2–4) were measured to obtain an average, and the value expressed as the average xylem area-specific lumen resistivity. This was multiplied by the vessel density to obtain the R_L of the average vessel. Previous work indicated the Hagen–Poiseuille value accurately estimates the actual lumen resistivity (Zwieniecki, Melcher & Holbrook 2001a; Sperry *et al*. 2005). The diameter of the average vessel was calculated from the average R_L according to the Hagen–Poiseuille equation.

The average end wall resistivity on a vessel basis (R_W) was calculated for each stem as the total resistivity minus the lumen resistivity ($R_W = R_C - R_L$). The fraction of the total resistivity in the end wall (F_W) was $F_W = R_W/R_C$ (Table 2). Each value (R_C, R_L, R_W, F_W) was determined for five to six stems per species, with the species being represented by the grand mean of each parameter.

End wall resistance (r_W)

According to the assumed vessel geometry (Fig. 1), $r_W = R_W L'$. To obtain L' we estimated the L'/L ratio and multiplied this by the average length L. To get L'/L we measured the 'length fraction' (Table 1), which was the length of a vessel in contact with other vessels relative to the total vessel length. One way to estimate this length fraction would be to serially section a vessel from end-to-end at regular length intervals, and note the fraction of the total number of sections that the vessel is not in contact with another one. This would approximate the fraction of the vessel length that was not in contact with adjacent vessels. One minus this quantity is the length fraction. Instead

of making serial sections, we assumed that the end walls were randomly distributed longitudinally. Accordingly, a single cross-section across all vessels will contain the equivalent of the serial sections arrayed in one plane. The length fraction was estimated from one cross-section as the ratio of solitary vessels to total vessel groupings, where the latter is the sum of solitary vessels and clusters of contiguous vessels (each cluster counting as 1).

The length fraction was estimated from counts of all vessel groupings in three radial sectors of xylem per stem. Each stem was represented by the mean of the three subsample fractions. The species was represented by the grand mean from the same six stems used in the other measurements. From the length fraction, the ratio L'/L was calculated as: $L'/L = 1 - (\text{length fraction})/2$ (Table 1). The length fraction is divided by 2 because we assumed that half of the total overlap per vessel was in one end wall. This assumes no lateral contact between adjacent files of vessels, and so our L' and r_W estimates represent maximum values for the vessel.

Area-specific pit resistance (r_P)

This was calculated as the product of the average end wall resistance and half of the average pit membrane area per vessel (A_P): $r_P = r_W A_P/2$ (Table 2). Half of the pit area was used because vessel efflux will be through just one end wall, the other half handling the influx through the other end wall (Fig. 1). The r_P represented the maximum for the vessel because its calculation assumed all pitting was in the end walls with none on lateral walls.

Determining the pit membrane area per vessel (A_P) began with measuring the 'contact fraction' which was the portion of the vessel wall area that is in pitted contact with other vessels (Table 1). Similar to the length fraction, the contact fraction could be determined from serial sections of a vessel at regular intervals, measuring in each section the perimeter of the vessel in contact with another as well as the total vessel perimeter. The contact fraction would be the sum of the contact perimeter across all sections over the sum of the total perimeter. Assuming that end-walls are randomly distributed, a single section across all vessels contains the equivalent of the serial sections for all vessels in one plane. The contact fraction was estimated from the ratio of contact perimeter to total perimeter, both being first summed across all vessels in section. The fraction represented an average for all vessel sizes in the section.

This fraction was estimated from perimeter measurements of all vessels in three radial sectors of xylem per stem. Each stem was represented by the mean of the three subsample fractions. The species was represented by the grand mean from the same six stems used in the other measurements.

Not all of the contact area between vessels is occupied by pits. In radial longitudinal sections of a subsample of the six stem segments we measured the total pit area per unit contact area. This 'pitfield fraction' (Table 1) was multiplied by the contact area fraction to obtain the average pit area per vessel area fraction (F_P). The average vessel area (A_V) was estimated from the average diameter and length for the species assuming cylindrical geometry. The total pit area per vessel was: $A_P = F_P A_V$ (Table 2).

Error propagation

Standard methods (Bernard & Epp 1995) were used to propagate standard errors from measured values (parameters R_C, R_L, R_W, L, length fraction, pitfield fraction, contact fraction) to calculated parameters (A_P, A_V, F_P, L'/L, r_P, r_W, F_W, average conduit diameter).

Pit aperture and membrane properties

In six species (*Amelanchier alnifolia*, *A. utahensis*, *Physocarpus malvaceus*, *Rubus parvifolius*, *R. leucodermis*, *Sorbus scopulina*) we further subdivided the total pit resistance into aperture and membrane components based on our previous pit modelling work (Sperry & Hacke 2004). Aperture resistance on a pit area basis was estimated from equation 20 in Sperry & Hacke (2004) using measurements of aperture diameter and thickness. Apertures were elliptical so we calculated their hydraulic diameter (the equivalent circle diameter giving the same Hagen–Poiseuille conductivity) from the long and short axis according to Lewis (1992). Membrane resistance on an area basis was calculated as the total pit resistance (r_P) minus the aperture resistance. From equation 17 in Sperry & Hacke (2004) we calculated the 'equivalent pore diameter' of the membrane from our measurement of the area-specific membrane resistance. The area-specific membrane resistance times the pore density gives the average resistance per membrane pore, the diameter of which is the equivalent pore diameter. Pore density was based on the membrane being composed of multiple sheets of parallel microfibrils superimposed as detailed in Sperry & Hacke (2004).

RESULTS

The xylem resistivity on a conduit area basis (R_{Ca}) increased significantly with increasing cavitation resistance over a P_{50} range from 0.76 to 6.66 MPa (Fig. 2) consistent with a safety versus efficiency trade-off at the whole conduit level. This trend was significant within the 11 Rosaceae species ($r^2 = 0.36$) and reinforced by the five additional species ($r^2 = 0.51$). The trend was also significant for vessel resistivity expressed on a total xylem area basis (not shown).

The increase in resistivity with P_{50} was nearly equally divided between lumen (R_L) and end wall (R_W) components (Fig. 3). The average wall resistivity fraction (F_W; see Table 2 for summary of symbols) was $53 \pm 3\%$, indicating that lumen and wall were approximately co-limiting. There was no significant trend in F_W with P_{50}, nor any difference between the average F_W for Rosaceae versus other species. This result means that any safety versus efficiency trade-off involved similar increases in both the end wall and lumen resistance.

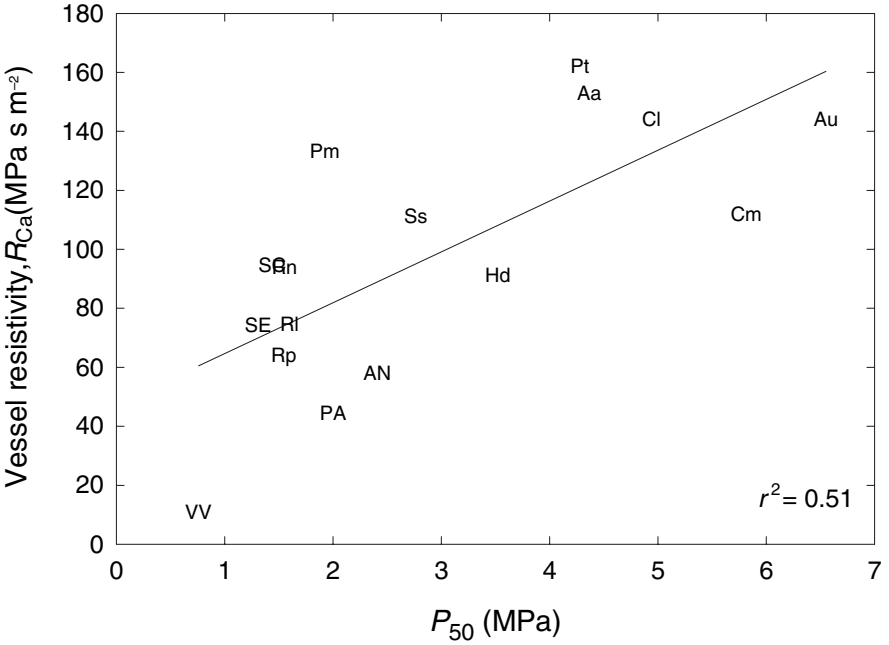

Figure 2. Vessel resistivity on a lumen cross-sectional area basis (R_{Ca}) versus P_{50}. The P_{50} is the absolute value of the negative pressure reducing 50% of the hydraulic conductivity. Greater resistance to cavitation (higher P_{50}) was associated with higher resistivity consistent with a safety versus efficiency trade-off. Mean values from five to six stems per species are shown without error bars for clarity. The average standard error as percentage of the mean was 10% for P_{50} and 15% for R_{Ca}. Symbols refer to species as listed in Table 1.

The increase in R_L with P_{50} resulted from a decline in average conduit diameter with P_{50} (Fig. 4a; symbols). What caused the increase in R_W with P_{50}? The R_W is the wall resistance (r_W) divided by the length L' (Fig. 1), so its increase could result from shorter length and/or higher r_W with P_{50}. There was no significant relationship between either L'/L (Table 1) or total vessel length (L) and P_{50} (Fig. 4b; symbols). There was, however, a significant increase in r_W with P_{50} (Fig. 5).

The increase in r_W could result from higher area-specific pit resistance (r_P) and/or lower pit area per vessel (A_P). We had hypothesized that r_P should increase with P_{50} because of the less porous pit membranes required to suppress cavitation by air-seeding. Although there was considerable variation in r_P, contrary to our expectations, a regression against P_{50} showed no relationship (see Table 1 for r_P values). The r_P was also just as variable in the Rosaceae as across the diversity of other families (Table 1). Instead, the increase in r_W was a result of dramatically less pit area per vessel with increased P_{50} (Fig. 6; solid regression). Pit surface area per vessel (A_P) declined in inverse proportion to increasing P_{50} both within the 11 Rosaceae ($r^2 = 0.62$) and for all species combined ($r^2 = 0.75$).

Total vessel surface area (A_V) also declined with increasing P_{50}, but not as steeply as pit area (Fig. 6; dashed regression). This was because the pit fraction (F_P; pit area per

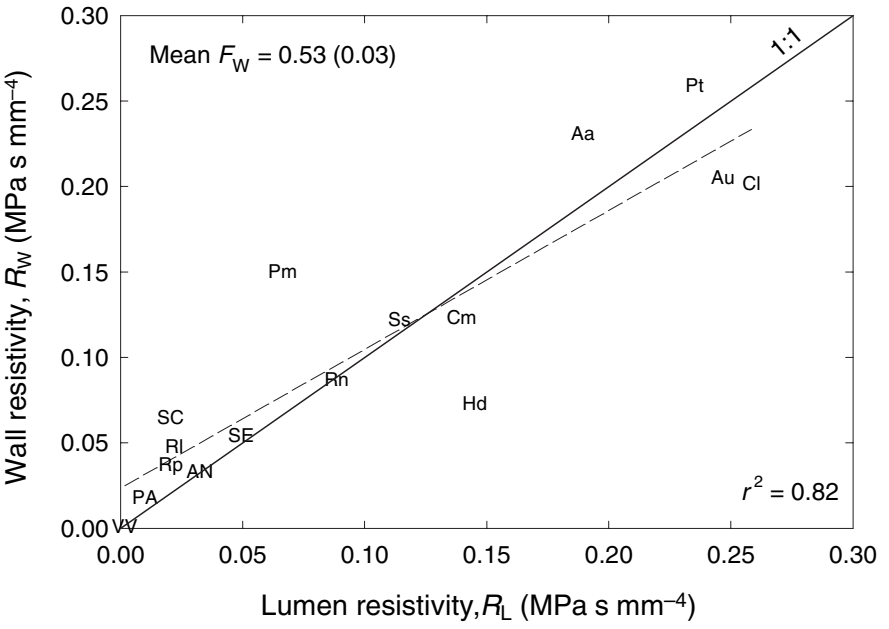

Figure 3. Lumen resistivity (R_L) versus end wall resistivity (R_W). Values are expressed on a vessel basis and the wide range reflects the variation in lumen size across the species. The data was close to the 1 : 1 line indicating that on average both resistivity components contribute equally to their sum, the total vessel resistivity (R_C). The average wall fraction ($F_W = R_W/R_C$) was 0.53 ± 0.03 across all species with no differences between Rosaceae versus others. Means of five to six stems per species are shown without error bars for readability. Average standard error as percentage of mean was 13% for R_L and 19% for R_W.

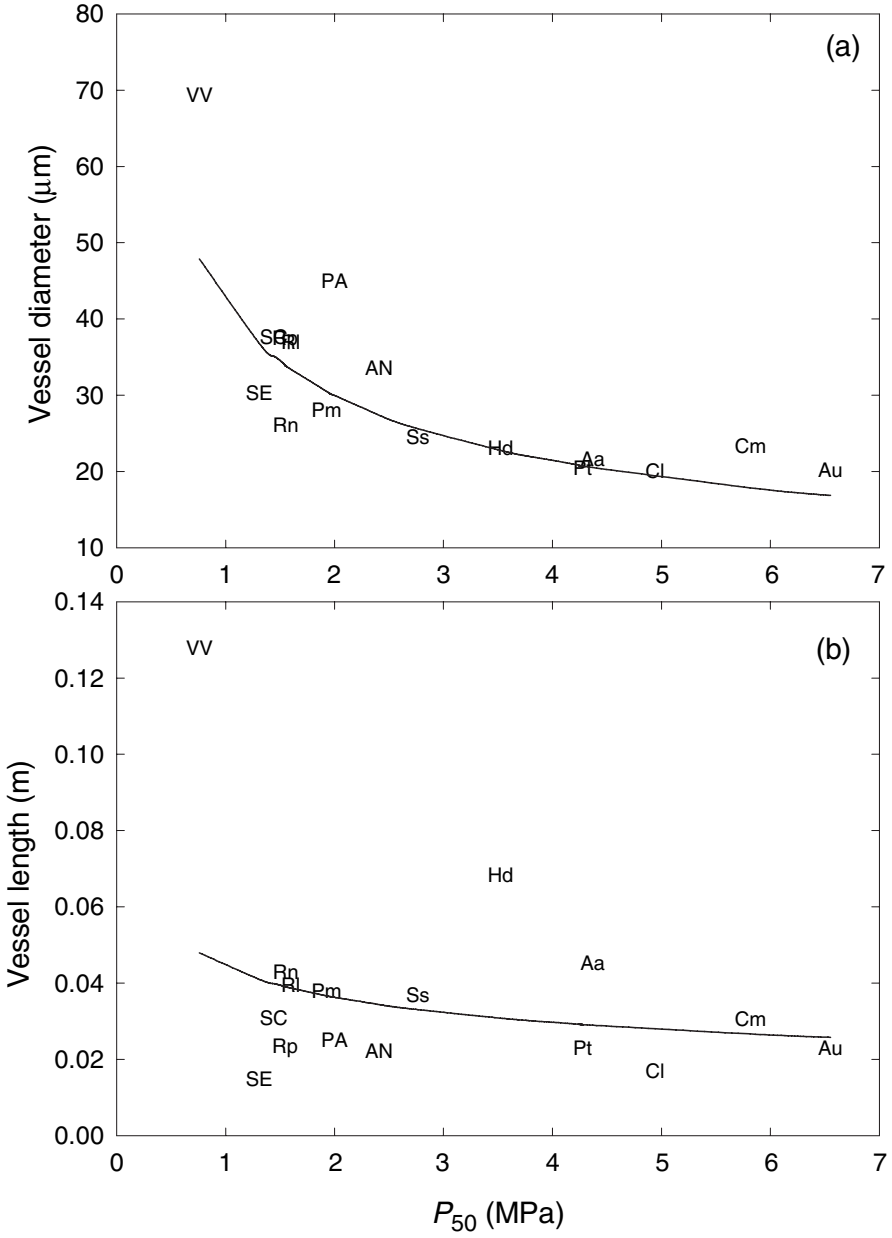

Figure 4. (a) Average vessel lumen diameter versus P_{50}. Symbols show means of five to six stems per species with the average diameter calculated from the average lumen resistivity (R_L). Error bars not shown for clarity, standard error averaged 7% of the mean for diameters. An inverse relationship between diameter and P_{50} (not shown) was significant (diameter = 44.6 $P_{50}^{-0.47}$, $r^2 = 0.72$). Curve is calculated assuming that P_{50} is controlled by total pit area per vessel according to the relationship in Fig. 6 with other parameters averaged except for the pit fraction (F_P) which declines with P_{50} as seen in Fig. 6 (see Appendix for summary calculations). (b) Average vessel length versus P_{50}. Symbols are log transformed means from three to seven stems per species, error bars not shown for clarity but the standard error averaged 7% of the mean for lengths. A linear relationship with P_{50} was not significant. Curve is calculated on same basis as in (a).

vessel area) decreased significantly with increasing cavitation resistance (Fig. 7). All pit fractions were very low, the highest being 15% declining to less than 2% for the most cavitation-resistant species. The low pit fractions were mostly a result of limited overlap between vessels (i.e. low contact fractions in Table 1) rather than sparse pitting at areas of overlap (i.e. relatively high pitfield fractions in Table 1).

The area-specific pit resistances were much higher than estimated from our pit model (Sperry & Hacke 2004). The model predicted a range from 0.2 to 20 MPa s m^{-1} (Fig. 9 in Sperry & Hacke 2004) whereas measured values averaged 167 MPa s m^{-1} excluding an extreme value for *Amelanchier alnifolia* (Table 1). Although the r_P estimates were the maximum in the absence of any lateral pitting and the error in its determination was relatively high because of the number of calculations required (average standard error was 29% of the mean, Table 1), it is unlikely that these factors accounted for the order-of-magnitude discrepancy. Aperture resistance accounted for 1% or less of the total pit resistance in the six species subsampled, indicating the model was under-estimating the membrane resistance. Membranes were much less porous than the model predicted. Equivalent pore diameters based on the measured membrane resistance ranged from 3.5 to 7.6 nm (mean = 5.3 nm). In contrast, the pore diameter expected to air-seed at the P_{50} values of these species ranged from 44 to 383 nm from the capillary equation (surface tension =0.073 Pa m).

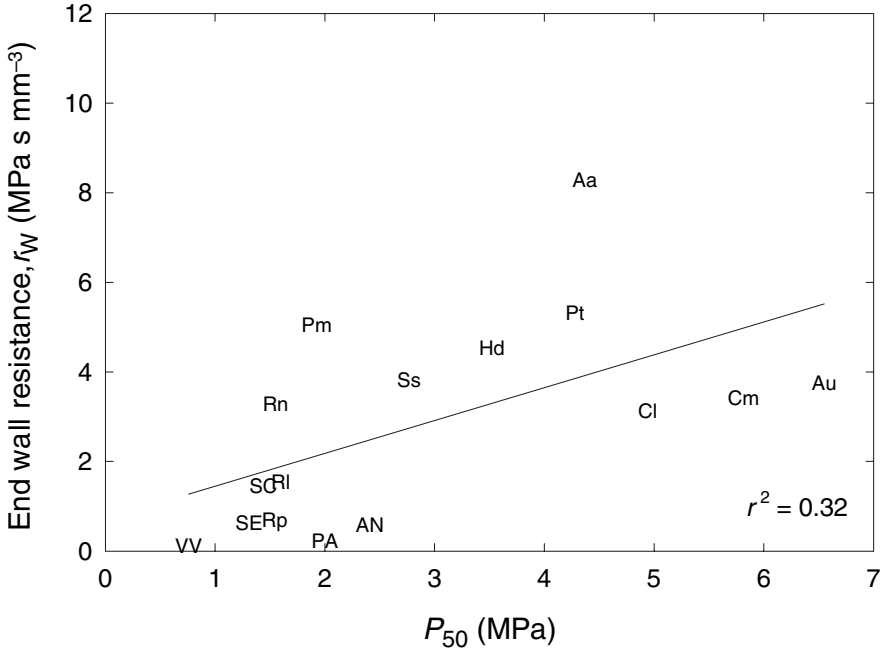

Figure 5. End wall resistance (r_W) versus P_{50}. Resistance increased significantly with P_{50}. Error bars not shown for clarity, but the standard error averaged 23% of the mean.

DISCUSSION

A proposed basis for a safety versus efficiency trade-off

The results did not support the expected trade-off between area-specific pit resistance and P_{50}. Although our measurement of r_P was an indirect and maximum estimate with inevitably high error (Table 1), the pit model predicted a 10-fold increase over the 6 MPa range in P_{50} in our study species (Sperry & Hacke 2004) whereas we observed no P_{50}-related variation. Apparently the majority of membrane pores were of similar size in all species and this size was not correlated with the largest pore causing air-seeding of cavitation. This was the same conclusion drawn by Choat and others from experimental estimates of membrane porosity (Choat *et al*. 2003, 2004). Either the air-seeding is caused by yielding or rupture of the pit membrane, or the largest pore that causes the air-seeding is relatively rare and not related to the prevailing porosity that determines membrane resistance.

In place of our rejected hypothesis the results suggest an alternative. The decline in total pit area per vessel with

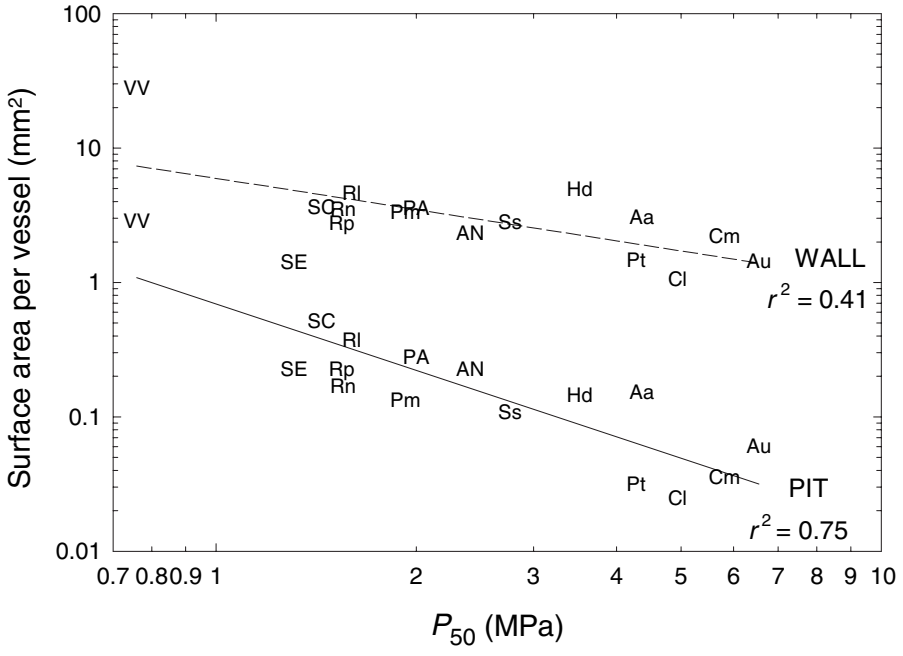

Figure 6. Total surface area of the average vessel (A_V, upper dashed 'WALL' regression) and total surface area of pits in the average vessel (A_P, lower solid 'PIT' regression) versus P_{50} on a log–log scale. Both declined significantly with P_{50}. The trade-off hypothesis assumes that total pit area per vessel determines the P_{50} by determining the average size of the largest membrane pore per vessel. The pit area is fitted well as an inverse function of P_{50}: $A_P = 0.69\ P_{50}^{-1.64}$ ($r^2 = 0.75$). Error bars not shown for clarity, standard error of A_V averaged 10% of the mean, and standard error of A_P averaged 15% of the mean.

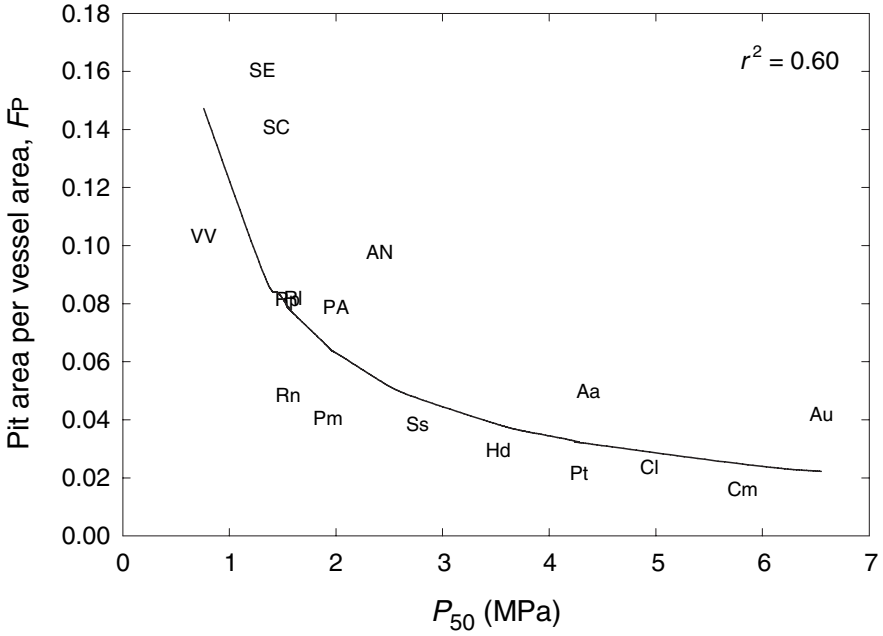

Figure 7. Pit surface area per total vessel surface area (F_P) versus P_{50}. The 'pit fraction' declined in inverse relation to P_{50}: $F_P = 0.116 P_{50}^{-0.88}$ ($r^2 = 0.60$). Error bars not shown for clarity, standard error of F_P averaged 11% of the mean.

increasing P_{50} (Fig. 6) suggests that it is the total area of pits in a vessel rather than individual pit structure that is most important in setting a vessel's cavitation resistance and transport efficiency. If the average size of the rare largest pore per vessel increases with total pit area per vessel, the capillary equation predicts an inverse relationship between total pit area and the average air-seeding pressure. Although the probability of mechanical failure might also increase with cumulative pit area, it is not clear why this should be an inverse relationship as was observed (Fig. 6). The most parsimonious explanation, and one offered previously by Choat *et al*. (2003, 2004) and Hargrave *et al*. (1994), is that safety from cavitation is determined by the rare largest membrane pore per vessel. We add the assumption that the average size of the largest pore per vessel increases with increasing total pit membrane area per vessel.

There is a basis for this assumption if there is a theoretical pore size distribution that is essentially common to all species with a homogenous type of pit membrane. Vessels with small total pit area represent this distribution with a small sample size. The average pore distribution for a small sample size will have a similar mean pore diameter and r_P as the theoretical distribution, but much smaller maximum pore size on average, and hence much greater average cavitation pressure (and P_{50}) according to the capillary equation. Vessels with increasingly larger total pit area sample more of the theoretical distribution, and while the mean pore size and r_P stays the same, the average maximum pore size will increase leading to lower average cavitation pressure (and P_{50}). Adding to this inherent vulnerability of vessels with large pit area is the fact that these vessels should also have a greater chance of contacting air-filled vessels.

According to this pore size scenario, species with the highest P_{50} values and hence the very smallest pit areas will have an average maximum pore size closer to the theoretical mean. The highest P_{50} in an angiosperm that we know of is 11.3 MPa in the desert shrub *Larrea tridentata* (Pockman & Sperry 2000). This corresponds to an average maximum pore diameter per vessel of 26 nm, which is approaching the 3–7 nm range predicted for the equivalent pore diameters and the range measured experimentally by others. Conversely, the lowest P_{50} in our data set was 0.76 MPa in *Vitis vinifera,* which also had the largest pit area per vessel (Fig. 5). This pressure corresponds to an average maximum pore size per vessel of 383 nm, which should be approaching the maximum of the theoretical pore distribution.

A causal relationship between pit area and cavitation pressure provides a relatively simple explanation for many of the results, beginning with the observation that wall and lumen resistivities are roughly co-limiting (Fig. 3). If a given level of safety from cavitation dictates a limited total pit area per vessel, and if the pit area fraction (F_P) is held constant, the total wall area of the vessel is also limited. If the total wall area of the vessel is limited, the product of length and diameter must be constant. Such a vessel can be long and narrow, or short and wide, but its surface area must be preserved. Solving for the wall resistivity fraction that minimizes the conduit area-specific resistivity (R_{Ca}) under this surface area constraint (Appendix) yields an optimal fraction of $F_W = 0.40$ (Fig. 8; conductivities = $1/R_{Ca}$ shown for illustrative purposes). The average wall fraction was higher at 0.53, but the breadth of the optimum is such that the species still achieved an average of 94 ± 2% of their maximum conductivity per conduit area (Fig. 8; symbols on curve).

The proposed trade-off also explains the rather low pit fractions (F_P) and their decrease with P_{50} (Fig. 7). A low F_P means a larger vessel for the same limiting total pit area. A

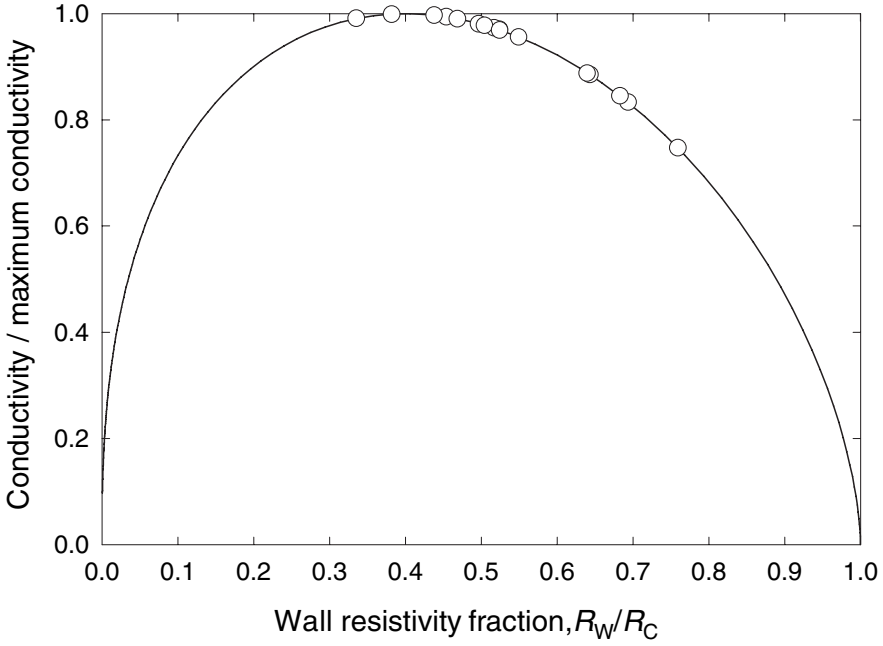

Figure 8. Conduit conductivity per cross-sectional lumen area relative to its maximum versus end wall resistivity fraction ($F_W = R_W/R_C$) calculated according to Eqn A8 (Appendix). Conductivities are shown rather than the reciprocal R_{Ca} to avoid infinite values at F_W extremes. The curve assumes a fixed vessel surface area so that diameter varies inversely with length. High F_W corresponds to a wide but short vessel, low F_W is a long but narrow vessel. Maximum conductivity per cross-sectional area occurs at $F_W = 0.4$. Observed wall fractions are indicated by symbols, and achieved an average of 94 ± 2% of the theoretical maximum.

larger vessel means a lower R_{Ca} (with the minimum still at $F_W = 0.4$). The decline in F_P with increasing P_{50} prevents total vessel size from decreasing as much as total pit area (Fig. 6) and keeps the conduit resistivity from increasing with P_{50} as much as it would if F_P were constant.

Most importantly, a pit area versus cavitation linkage explains the tendency for conduit resistivity to increase with P_{50} (Fig. 2). Assuming the inverse relationship between total pit area and P_{50} (Fig. 6), incorporating the observed relationship between pit fraction (F_P) with P_{50} (Fig. 7), and using average values for area-specific pit resistance ($r_P = 167$ MPa s m^{-1}), wall fraction ($F_w = 0.53$), and L'/L (0.82), the total conduit resistivity increases with P_{50} much as observed (Fig. 9; 'observed F_P trend' line versus data regression, see Appendix for calculations). The remaining discrepancies are owing to variation in the actual values of F_P, F_W, L'/L, and r_P around their average. The compensating effect of decreased pit fraction (F_P) in more resistant species is demonstrated by holding this value constant at its maximum (0.15) and observing how much more steeply the conduit resistivity increases with P_{50} (Fig. 9; 'constant F_P' line). Theoretically, a reduction in F_P with increasing P_{50} can completely eliminate the safety versus efficiency trade-off, but this requires F_P to drop drastically to below 0.05%. The disadvantage of extremely low pit fractions would be much higher lateral flow resistance (Orians *et al*. 2004), a problem that probably limits how much F_P can drop and still benefit the plant.

The trade-off is also consistent with vessel diameter being more sensitive to P_{50} than length (Fig. 4). The solid curves in Fig. 4 are the diameter and length of the vessels having resistivities plotted in Fig. 9 assuming the observed trend in pit fraction and setting other parameters to their averages (Fig. 9; 'observed F_P trend' line, Appendix). Diameter drops by almost three-fold over the P_{50} range whereas length drops by just over 1.5-fold.

Finally, the variable relationship between diameter, length and overall resistivity with P_{50} (Figs 2 & 4) is accommodated by the trade-off hypothesis. The variation is primarily a result of variation in F_P, F_W, L'/L, and r_P – none of which are mechanistically linked to P_{50}, which is set only by total pit area. The greater scatter in the insignificant length versus P_{50} data (Fig. 4b) versus the significant diameter versus P_{50} relationship (Fig. 4a) is because length is more sensitive to variation in F_P than diameter (Appendix). As a result of these interactions, there was no prevailing allometry between length and diameter across the 16 species as opposed to our earlier more limited survey that suggested that length scaled with the square of the diameter (Sperry *et al*. 2005). In summary, a single P_{50} can be associated with a number of different vessel sizes and resistivities depending on variation in F_P, F_W, L'/L, and r_P. Nevertheless, the need to reduce pit area per vessel to achieve greater safety from cavitation is proposed to drive the general trend toward less efficient xylem transport seen over broad ranges in P_{50}.

General discussion

The safety versus efficiency trade-off that we propose is quite different from what we expected. We had thought that plants acquired greater safety from cavitation by making denser pit membranes that were less porous on average and so with higher flow resistance. Instead, the results show that average pit membrane porosity and flow resistance does not vary systematically with cavitation resistance in the study species. These plants may be achieving greater safety by reducing the pit area per conduit and thus by chance

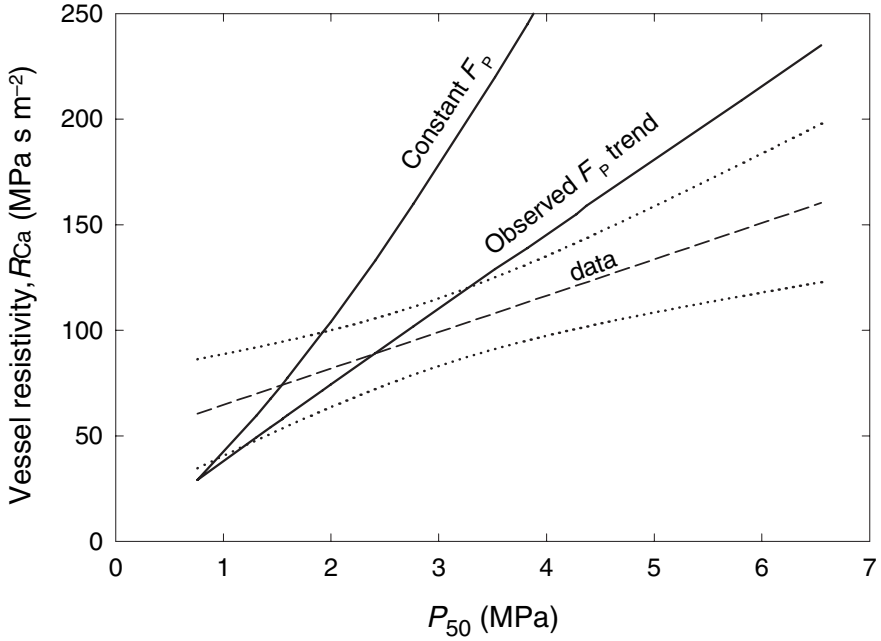

Figure 9. Vessel resistivity on a cross-sectional lumen area basis (R_{Ca}) versus P_{50}. The dashed data regression with 95% confidence limits is from the data in Fig. 2. The solid curves are all calculated assuming that P_{50} is determined by the total pit area per vessel according to the relationship in Fig. 6 and in Eqn A8 (Appendix). The 'observed F_P trend' line assumes the pit fraction (F_P) curve from Fig. 7. The 'constant F_P' line assumes F_P is constant at its maximum of 0.15. Other parameters were held constant at the average for the data set.

reducing the average size of the largest pore per conduit, which sets the air-seed pressure. Although the plant cannot control the cavitation pressure of a single conduit in this way, it can control the average response of the typically large population of conduits on which it depends. The trade-off with decreased transport efficiency results from the higher resistance of having less total pit area, and from the fact that a limited total pit area ultimately tends to limit the total size of the conduit.

The relatively small size of the majority of pores appears to be controlled by the hemicelluloses and pectins and other matrix components that constitute the 'filler' between the strength-providing cellulose microfibrils of the membrane (Dickson 2000; Choat *et al*. 2003). Because of this filler, membrane strength is not necessarily coupled to porosity as assumed in our model of homogenous pit membranes. The large variation in area-specific pit resistance that we measured (Table 1) and that was nevertheless not related to cavitation resistance may result from variation in the state of the matrix filler between species. Variation in xylem conductivity with ionic strength of the sap has been attributed to change in hydration of the matrix and hence pore size (Zimmermann 1983; Zwieniecki *et al*. 2001b). Based on limited observations with one species (*Acer negundo*), sap ionic strength does not alter the P_{50} (V. Stiller, J. Sperry, unpubl. data). Perhaps the treatment affects the majority of small pores more than the largest pore, leaving cavitation pressure unaltered.

The tendency for lumen and end wall resistivity to be co-limiting in plants (Fig. 3) was difficult to account for under our original hypothesis because it put no limit on vessel size with P_{50}. Large, safe vessels with large total pit area would be possible if the pit membrane porosity was as tightly controlled as we had originally assumed. Such vessels could be sufficiently long to reduce wall resistivity to a small percentage (Sperry & Hacke 2004; Sperry *et al*. 2005). The new trade-off hypothesis does limit vessel size to within the bounds of the minimum permissible pit area per vessel area fraction (F_P). A limit on vessel size results in the minimum resistivity being a compromise between reducing lumen resistivity with wide but short vessels versus reducing wall resistivity with long but narrow ones (Fig. 8).

The hydraulic trade-off we propose here is reinforced by a mechanical trade-off. The mechanical problem of achieving greater safety from cavitation is that it requires a thicker wall for a given diameter to withstand compressive forces and implosion. A greater wall thickness per diameter can translate to higher wood density, particularly where conduits make up a significant portion of the wood volume (Hacke *et al*. 2001). Higher density represents greater cost of wood growth per volume. A thicker wall per diameter also increases the hydraulic resistivity on an area basis even if there is no change in lumen diameter. A limitation on maximum wall thickness can potentially limit maximum diameter independently of purely hydraulic considerations.

Trade-offs result in a strong selective advantage to mechanisms that at least partially circumvent or resolve the conflict. We have already drawn attention to the advantage of minimizing the pit area per vessel area fraction (F_P), particularly as the P_{50} is increased in safer xylem (Figs 7 and 9). Variation in F_P provides an explanation for why there is no 1 : 1 relationship between vessel size and vulnerability – big vessels can be safe from cavitation, but only by reducing their F_P to keep their pit area small. There are other candidate mechanisms. The pit area that is presumably influencing the cavitation pressure is the pit area responsible for the capillary sealing of the pit membrane. Any mechanism that reduces the actual sealing area of the membrane relative to the total conducting area will mitigate the trade-off. Pit aspiration is a simple mechanism – if capillary forces are

sufficient to displace the membrane against the chamber wall, only the part of the membrane spanning the aperture is responsible for bearing the full brunt of the air–water pressure difference in a sealed pit. Vestured pits could work in the same way – water could be flowing through the entire membrane, but in the sealing position much of the membrane would be deflected against the vestures, reducing the area involved in sealing off air.

Tighter control over membrane pore size and distribution would have a tremendous advantage, as we had initially hypothesized, because total pit area could become less tightly coupled with vulnerability to cavitation. Although we did not see evidence for this in our limited sample, not all angiosperm pit membranes need be the same. Although the membrane porosity studies cited above (Choat *et al*. 2003, 2004) show no relationship with air-seeding pressure, similar methods applied to different species have shown correspondence between membrane pore size and cavitation (Jarbeau, Ewers & Davis 1995). Certainly some angiosperm pits are quite different in having a torus that may function like a conifer pit (Wheeler 1983; Jansen *et al*. 2004). In conifers, the dense torus seals the pit, allowing the pores of the surrounding margo to be quite large and conductive without sacrificing safety. Air-seeding occurs by slippage of the torus, and in theory is a function of individual pit membrane strength and structure (Hacke, Sperry & Pittermann 2004) rather than total pit area. Given the potential diversity in pit function it is unlikely that there will be a single structural basis for cavitation pressure across vascular plants.

ACKNOWLEDGMENTS

Funding was provided from National Science Foundation grants IBN-0112213 and IBN-0416297. The authors thank two anonymous reviewers whose thoughtful comments helped to improve the manuscript.

REFERENCES

Alder N.N., Pockman W.T., Sperry J.S. & Nuismer S. (1997) Use of centrifugal force in the study of xylem cavitation. *Journal of Experimental Botany* **48,** 665–674.

André J.-P. (2002) *Organisation Vasculaire Des Angiospermes: une Vision Nouvelle*. INRA, Paris, France.

Bernard C. & Epp C. (1995) *Laboratory Experiments in College Physics*. John Wiley & Sons, New York, USA.

Choat B., Ball M., Luly J. & Holtum J. (2003) Pit membrane porosity and water stress-induced cavitation in four co-existing dry rainforest tree species. *Plant Physiology* **131,** 41–48.

Choat B., Jansen S., Zwieniecki M.A., Smets E. & Holbrook N.M. (2004) Changes in pit membrane porosity due to deflection and stretching: the role of vestured pits. *Journal of Experimental Botany* **55,** 1569–1575.

Cochard H., Cruiziat P. & Tyree M.T. (1992) Use of positive pressures to establish vulnerability curves: Further support for the air-seeding hypothesis and implications for pressure-volume analysis. *Plant Physiology* **100,** 205–209.

Cohen S., Bennink J.P. & Tyree M.T. (2003) Air method measurements of apple vessel length distributions with improved apparatus and theory. *Journal of Experimental Botany* **54,** 1889–1897.

Crombie D.S., Hipkins M.F. & Milburn J.A. (1985) Gas penetration of pit membranes in the xylem of *Rhododendron* as the cause of acoustically detectable sap cavitation. *Australian Journal of Plant Physiology* **12,** 445–454.

Davis S.D., Ewers F.W., Wood J., Reeves J.J. & Kolb K.J. (1999) Differential susceptibility to xylem cavitation among three pairs of Ceanothus species in the Transverse Mountain ranges of Southern California. *Ecoscience* **6,** 180–186.

Dickson W. (2000) *Integrative Plant Anatomy*. Academic Press, San Diego, CA, USA.

Ewers F.W. (1985) Xylem structure and water conduction in conifer trees, dicot trees, and lianas. *International Association of Wood Anatomists Bulletin* **6,** 309–317.

Hacke U.G. & Sperry J.S. (2001) Functional and ecological xylem anatomy. *Perspectives in Plant Ecology, Evolution and Systematics* **4,** 97–115.

Hacke U.G., Sperry J.S. & Pittermann J. (2000) Drought experience and cavitation resistance in six desert shrubs of the Great Basin, Utah. *Basic and Applied Ecology* **1,** 31–41.

Hacke U.G., Sperry J.S. & Pittermann J. (2004) Analysis of circular bordered pit function. II. Gymnosperm tracheids with torus-margo pit membranes. *American Journal of Botany* **91,** 386–400.

Hacke U.G., Sperry J.S., Pockman W.P., Davis S.D. & McCulloh K.A. (2001) Trends in wood density and structure are linked to prevention of xylem implosion by negative pressure. *Oecologia* **126,** 457–461.

Hargrave K.R., Kolb K.J., Ewers F.W. & Davis S.D. (1994) Conduit diameter and drought-induced embolism in *Salvia mellifera* Greene (Labiatae). *New Phytologist* **126,** 695–705.

Ieperen W.V., Meeteren U.V. & Gelder H.V. (2000) Fluid ionic composition influences hydraulic conductance of xylem conduits. *Journal of Experimental Botany* **51,** 769–776.

Jansen S., Choat B., Vinckier S., Lens F., Schols P. & Smets E. (2004) Intervascular pit membranes with a torus in the wood of Ulmus (Ulmaceae) and related genera. *New Phytologist* **163,** 51–59.

Jarbeau J.A., Ewers F.W. & Davis S.D. (1995) The mechanism of water-stress-induced embolism in two species of chaparral shrubs. *Plant, Cell and Environment* **18,** 189–196.

Lancashire J.R. & Ennos A.R. (2002) Modelling the hydrodynamic resistance of bordered pits. *Journal of Experimental Botany* **53,** 1485–1493.

Lewis A.M. (1992) Measuring the hydraulic diameter of a pore or conduit. *American Journal of Botany* **79,** 1158–1161.

Martinez-Vilalta J., Prat E., Oliveras I. & Pinol J. (2002) Xylem hydraulic properties of roots and stems of nine Mediterranean woody species. *Oecologia* **133,** 19–29.

Neufeld H.S., Grantz D.A., Meinzer F.C., Goldstein G., Crisosto G.M. & Crisosto C. (1992) Genotypic variability in vulnerability of leaf xylem to cavitation in water-stressed and well-irrigated sugarcane. *Plant Physiology* **100,** 1020–1028.

Orians C., van Vuuren M., Harris N., Babst B. & Ellmore G. (2004) Differential sectoriality in long-distance transport in temperate tree species: evidence from dye flow, 15N transport, and vessel element pitting. *Trees – Structure and Function* **18,** 501–509.

Pittermann J. & Sperry J.S. (2003) Tracheid diameter determines the extent of freeze-thaw induced cavitation in conifers. *Tree Physiology* **23,** 907–914.

Pockman W.T. & Sperry J.S. (2000) Vulnerability to xylem cavitation and the distribution of Sonoran Desert vegetation. *American Journal of Botany* **87,** 1287–1299.

Salleo S., Lo Gullo M.A., De Paoli D. & Zippo M. (1996) Xylem recovery from cavitation-induced embolism in young plants of

Laurus nobilis: a possible mechanism. *New Phytologist* **132,** 47–56.
Schulte P.J. & Gibson A.C. (1988) Hydraulic conductance and tracheid anatomy in six species of extant seed plants. *Canadian Journal of Botany* **66,** 1073–1079.
Sperry J.S. (1995) Limitations on stem water transport and their consequences. In: *Plant Stems: Physiology and Functional Morphology* (ed. B.L. Gartner), pp. 105–124. Academic Press.
Sperry J.S. & Hacke U.G. (2004) Analysis of circular bordered pit function. I. Angiosperm vessels with homogenous pit membranes. *American Journal of Botany* **91,** 369–385.
Sperry J.S., Hacke U.G. & Wheeler J.K. (2005) Comparative analysis of end wall resistance in xylem conduits. *Plant, Cell and Environment* doi: 10.1111/j.1365-3040.2005.01287.
Sperry J.S., Saliendra N.Z., Pockman W.T., Cochard H., Cruiziat P., Davis S.D., Ewers F.W. & Tyree M.T. (1996) New evidence for large negative xylem pressures and their measurement by the pressure chamber method. *Plant, Cell and Environment* **19,** 427–436.
Tyree M., Davis S. & Cochard H. (1994) Biophysical perspectives of xylem evolution – is there a tradeoff of hydraulic efficiency for vulnerability to dysfunction? *IAWA Journal* **15,** 335–360.
Wheeler E.A. (1983) Intervascular pit membranes in Ulmus and Celtis native to the USA. *IAWA Bulletin* **4,** 79–88.
Zimmermann M.H. (1983) *Xylem Structure and the Ascent of Sap*. Springer-Verlag, Berlin, Germany.
Zimmermann M.H. & Jeje A.A. (1981) Vessel length distribution of some American woody plants. *Canadian Journal of Botany* **59,** 1882–1892.
Zwieniecki M.A., Melcher P.J. & Holbrook N.M. (2001a) Hydraulic properties of individual xylem vessels of *Fraxinus americana*. *Journal of Experimental Botany* **52,** 257–264.
Zwieniecki M.A., Melcher P.J. & Holbrook N.M. (2001b) Hydrogel control of xylem hydraulic resistance in plants. *Science* **291,** 1059–1062.

Received 15 November 2004; received in revised form 6 January 2005; accepted for publication 13 January 2005

APPENDIX

Calculation of end wall and pit resistances

Assuming the vessel geometry diagrammed in Fig. 1 with lumen and wall components in series, vessel $R_C = R_L + R_W$. In terms of vessel diameter and length (D, L)

$$R_C = 128\ \eta/(\pi D^4) + r_W/(LF_L) \quad \text{(A1)}$$

where η is viscosity, r_W is the resistance of one end-wall, and F_L is the ratio L'/L (Fig. 1). By measuring R_C, D, L, and F_L for the average-sized vessel as described in Materials and Methods we solved Eqn A1 for r_W. The pit resistance on a pit membrane area basis (r_P) was calculated as

$$r_P = r_W A_P/2 \quad \text{(A2)}$$

where A_P is the total pit membrane area per vessel. This assumes all pit area is located on vessel end walls as opposed to side walls, and that one end wall contains half of the total pit area. The A_P was calculated from

$$A_P = \pi D L F_P \quad \text{(A3)}$$

where F_P is the fraction of the vessel surface area occupied by pit membranes measured from wood sections as described.

Vessel resistivity (R_C) as a function of A_P

The proposed safety versus efficiency trade-off assumes that P_{50} is determined by A_P (Fig. 6). The ramifications for R_C can be explored by expressing Eqn A1 in terms of A_P rather than D and L. Efficiency is best expressed as R_C on a cross-sectional area basis (R_{Ca}), so each resistivity in Eqn A1 was multiplied by the lumen cross-sectional area. To eliminate D in this version of Eqn A1 we solved Eqn A3 for D [$D = A_P/(F_P \pi L)$] and substituted. This gives

$$R_L = 32\eta(\pi L F_P/A_P)^2 \quad \text{(A4)}$$

$$R_W = r_P A_P/(2\pi L^3 F_L F_P^2) \quad \text{(A5).}$$

To eliminate L we make use of the wall fraction (F_W) in terms of R_L and R_W

$$R_L/R_W = (1/F_w - 1) \quad \text{(A6)}$$

Substituting Eqns A4 and A5 for R_L and R_W in Eqn (A6) and solving for L yields

$$L = [(1/F_W - 1) r_P/(64\eta F_L)]^{1/5}\ (A_P/\pi)^{3/5}\ F_P^{-4/5} \quad \text{(A7).}$$

Plugging Eqn A7 into Eqns A4 and A5 and summing to get R_{Ca} results in the following summary equation for R_{Ca} on a cross-sectional area basis

$$R_{Ca} = 6.06(\pi/A_P)^{4/5}\eta^{3/5}(F_P r_P/F_L)^{2/5}[(1/F_W - 1)^{2/5} + (F_W/(1 - F_W))^{3/5}] \quad \text{(A8).}$$

This equation is graphed with respect to F_W in Fig. 8, showing that the minimum R_{Ca} (maximum conductivity per area) occurs at $F_W = 0.40$ when other parameters are constant. Figure 9 shows R_{Ca} calculated from Eqn A8 using mean values of r_P, F_L, F_W and assuming A_P varies with P_{50} as in Fig. 6. The F_P was assumed either to vary with P_{50} as in Fig. 7 (Fig. 9, observed F_P trend), or to remain constant (Fig. 9, constant F_P).

A final equation gives D as a function of A_P by substituting Eqn A7 for L into Eqn A3 and solving for D

$$D = [((F_W - 1)/F_W)\ 64\eta F_L/(r_P F_P)]^{1/5}\ (A_P/\pi)^{2/5} \quad \text{(A9).}$$

The curves in Fig. 4 show that for the observed decline in A_P and F_P with P_{50}, D decreases more than L (calculated from Eqns. A7 and A9 using mean values for the other parameters). Length is more sensitive to variation in F_P than D (compare Eqns. A7 and A9), consistent with the greater scatter in the L versus P_{50} relationship in Fig. 4b.